"Majority Representation" of Alloy Electronic States

L.-W. Wang, L. Bellaiche, S.-H. Wei, and A. Zunger
National Renewable Energy Laboratory, Golden, Colorado 80401
(Received 9 October 1997)

Despite the lack of translational symmetry in random substitutional alloys, their description in terms of single Bloch states has been used in most phenomenological models and spectroscopic practices. We present a new way of analyzing the alloy electronic structures based on a "majority representation" phenomenon of the reciprocal space spectrum $P(\mathbf{k})$ of the wave function. This analysis provides a quantitative answer to the questions: When can an alloy state be classified according to the crystal Bloch state symmetry, and under what circumstances are the conventional theoretical alloy models applicable. [S0031-9007(98)06043-8]

PACS numbers: 71.20.–b, 71.23.An, 78.20.Bh

Random substitutional $A_{1-x}B_x$ alloys lack translational symmetry both on the atomistic scale (due to random substitution of lattice sites by A and B atoms), and on the mesoscopic scale (due to statistical composition fluctuations leading to locally A-rich and B-rich regions). In semiconductor alloys, such loss of translational symmetry leads to scattering, manifested by a precipitous drop in carrier mobility [1], to exciton trapping, leading to the temperature dependence of photoluminescence (PL) lifetime and intensity [2–4], and to the appearance, in nominally indirect band-gap alloys, of direct transitions without phonon intervention [5]. Despite the formal illegitimacy of using physical concepts based on translational invariance when discussing random alloys, there is a strong tradition to do so in many phenomenological descriptions of alloy systems [6]. For example, reflectivity and PL peaks of alloys are routinely [7] classified in terms of Bloch-like van Hove singularities. Indeed, in many cases the identity of the translationally invariant states of pure crystals seems to be inexplicably preserved in random substitutional alloys. This point of view was carried out to its extreme in the widely used [6] "virtual crystal approximation" (VCA) [8–10], in which the symmetry of the alloy is assumed *identical* to the (higher) symmetry of the constituents. Thus, one needs to find a way to quantify the degree of translational symmetry in an alloy wave function. This will also help to classify different alloy systems according to this degree of translational symmetry and to judge the validity of various theoretical models (e.g., VCA, small supercells) that assume a certain level of translational symmetry.

If an alloy eigenfunction ψ_i were available, the extent of effective translational invariance could be quantified by expanding $\psi_i(\mathbf{r})$ in a complete set of Bloch functions $\{u_{n\mathbf{k}}(\mathbf{r})e^{i\mathbf{k}\cdot\mathbf{r}}\}$ of band index n and computing the sum over bands of the projection at a given translationally invariant wave vector $\mathbf{k}$ [which is inside the first Brillouin zone (BZ) of the constituent solid A and B]:

$$P_i(\mathbf{k}) = \sum_{n=1}^{\infty} |\langle \psi_i(\mathbf{r}) \,|\, u_{n\mathbf{k}}(\mathbf{r})e^{i\mathbf{k}\cdot\mathbf{r}}\rangle|^2. \qquad (1)$$

The alloy could be represented by a periodic supercell containing N atoms. The real alloy is then sought by increasing $N \to \infty$. For a given supercell, $\mathbf{k}$ is the reciprocal lattice vector of the supercell. If the alloy state ψ_i were dominated by a single "majority representation" (MR) wave vector $\mathbf{k}_{\mathrm{MR}}$, then $P_i(\mathbf{k}_{\mathrm{MR}}) \approx 1$ and $P_i(\mathbf{k})$ vs $\mathbf{k}$ will have a δ-like peak at $\mathbf{k} = \mathbf{k}_{\mathrm{MR}}$. In this case, the alloy wave function behaves essentially as a Bloch periodic state with wave vector $\mathbf{k}_{\mathrm{MR}}$. "Composition fluctuation" [3,4], manifested by the localization of ψ_i in a real-space domain rich in the low potential alloy constituent, would then lead to a broadening of this δ peak in $P_i(\mathbf{k})$. On the other hand, if no such majority representation wave vector $\mathbf{k}_{\mathrm{MR}}$ exists, we expect that $P_i(\mathbf{k}) \approx 0$ for all wave vector $\mathbf{k}$'s for large supercells.

A direct answer to these questions requires knowledge of the explicit single-particle *eigenstate* $\psi_i(\mathbf{r})$ of the random alloy. Unfortunately, contemporary theories such as the "averaged Green's function" [11] and the "coherent potential approximation" (CPA) [12], or "virtual crystal approximation" [8] and perturbation treatment based on it [13], provide only statistically averaged quantities, rather than explicit eigenstates. Indeed, a calculation of $\psi_i(\mathbf{r})$ requires a supercell that is large enough to capture localization due to composition fluctuation. For conventional semiconductor alloys, this entails $N \approx 10^3$–10^6 atoms. Because of advances in the computational algorithm for the electronic structure of large systems [14,15], it is now possible to calculate the band edge states for such large systems using atomistic screened pseudopotentials and plane wave basis functions [16].

We study substitutional binary semiconductor alloys made of zinc blende constituents: GaAs-AlAs, GaAs-InAs, GaAs-GaN, and GaP-GaN. The choice of these systems is based on the need to represent the major prototype behaviors: The lattice mismatch between GaAs and AlAs is very small (thus, the effect of atomic relaxation is negligible), while the lattice mismatch is significant in GaAs-InAs (7%) and huge in GaAs-GaN and GaP-GaN ($\sim$20%). Furthermore, while GaAs-AlAs and GaAs-InAs represent mixing on the cation sublattice, GaAs-GaN and

GaP-GaN represent anion mixing. Also, $GaAs_{1-x}N_x$ and $GaP_{1-x}N_x$ have resonant or bound impurity states at $x \to 0$ and $x \to 1$ limits [17], while in the other alloys, there is no such impurity levels in the dilute limits.

To model a random alloy, we have used $(001) \times (010) \times (100)$ cubic supercells containing $N = 512$, 4096, and 32 768 atoms for $P_i(\mathbf{k})$ calculation, and $N = 2 \times 10^6$ atoms for calculating the localization due to composition fluctuation. The atoms are assigned randomly to the ideal zinc blende lattice sites. We then used the "valence force field" [18] method to displace the atoms to the minimum strain energy positions. The Hamiltonian of the relaxed supercell is written as $\hat{H} = -\frac{1}{2}\nabla^2 + \sum_\alpha \sum_{\mathbf{R}_\alpha} v_\alpha(|\mathbf{r} - \mathbf{R}_\alpha|)$, where α is the type of the atom located at $\mathbf{R}_\alpha$, and v_α is the empirical screened pseudopotential of atom type α fitted [16,17,19] to the constituent bulk band structures, effective masses, and deformation potentials. We study the band edge states [valence band maximum (VBM) and conduction band minimum (CBM)], since they are involved in carrier dynamics and photoluminescence. For systems with up to ~30 000 atoms, the band edge states are calculated using the folded spectrum method [14]. For systems containing millions of atoms, a linear combination of bulk band [15] method is used to generate the approximated eigenstates. After determining the variational expansion coefficients $C_i(\mathbf{q})$ of $\psi_i(\mathbf{r})$ in terms of the plane wave basis function $e^{i\mathbf{q}\cdot\mathbf{r}}$, the projection of Eq. (1) is evaluated as $P_i(\mathbf{k}) = \sum_{\mathbf{G}} |C_i(\mathbf{k} + \mathbf{G})|^2$, here $\mathbf{G} = \mathbf{q} - \mathbf{k}$ is the reciprocal lattice vector of the zinc blende primary cell. We find four classes of behavior for the alloy band edge state ψ_i, illustrated in Figs. 1–4, respectively.

(i) *Strong majority representation: The CBM of GaAlAs and GaInAs.*—Figure 1 shows $\psi^2_{\mathrm{CBM}}(\mathbf{r})$ and $P_{\mathrm{CBM}}(\mathbf{k})$ for the direct gap, lattice matched $Ga_{0.7}Al_{0.3}As$ alloy. In real space, $\psi^2_{\mathrm{CBM}}(\mathbf{r})$ looks like a crystal Bloch state. This is corroborated in reciprocal space by the fact that there is a single dominant $\mathbf{k}$ point ($\mathbf{k}_{\mathrm{MR}} = \Gamma$) which contains 90% of the total spectral weight of $P_i(\mathbf{k})$. As shown in Fig. 1 and Table I, this weight at $\mathbf{k}_{\mathrm{MR}}$ is roughly a constant when the size of the supercell increases, while the weight on the other $\mathbf{k}$ points drops. This distinguishes this majority representation point $\mathbf{k}_{\mathrm{MR}}$ from all other $\mathbf{k}$ points. In our calculation scheme, $\mathbf{k}$ is discrete due to the use of a supercell. We can define, however, a spectrum $Q_i(\kappa)$ with a continuous variable κ

$$Q_i(\kappa) = \lim_{L\to\infty} \sum_{\mathbf{k}} w(\mathbf{k} - \kappa; L) P_i(\mathbf{k}), \qquad (2)$$

where $w(\mathbf{k} - \kappa; L)$ is a normalized broadening function, with width $\propto 1/L$ where L is the length of the cubic supercell. Note that $\int_{\mathrm{BZ}} Q_i(\kappa) d^3\kappa = 1$ due to $\sum_{\mathbf{k}} P_i(\mathbf{k}) = 1$, and that for $\mathbf{k} \neq \mathbf{k}_{\mathrm{MR}}$, each $P_i(\mathbf{k})$ goes to zero as $1/N$ when $L \to \infty$, but $Q_i(\kappa)$ is finite due to the normalization procedure of Eq. (2). Figure 1 shows that if the trend in panels (a), (b), and (c) will continue to an infinite supercell, $Q_i(\kappa)$ will contain a finite, smooth background function and a δ function at the majority representation point $\mathbf{k}_{\mathrm{MR}}$. The situation is similar for the CBM of $Ga_{0.5}In_{0.5}As$ (Table I), despite the 7% lattice mismatch. For the indirect gap alloy $Ga_{0.4}Al_{0.6}As$, we find that the $\mathbf{k}_{\mathrm{MR}}$ of CBM is at the X point, and $P_{\mathrm{CBM}}(\mathbf{k}_{\mathrm{MR}}) \approx 0.98$ (Table I).

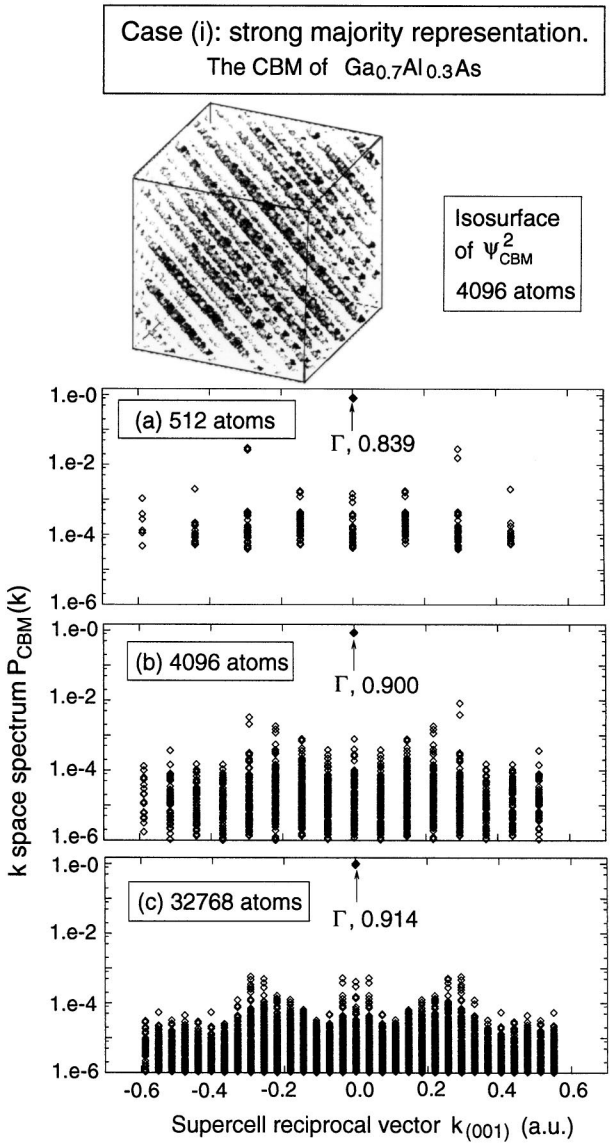

FIG. 1. Real-space isosurface (encompassing 30% of the total charge) and reciprocal-space spectral for the conduction band minimum state of $Ga_{0.7}Al_{0.3}As$. Each diamond symbol represents one $P_{\mathrm{CBM}}(\mathbf{k})$ vs $\mathbf{k}$ point.

(ii) *Weak majority representation: The CBM of GaAsN and GaPN.*—In these alloys, the chemical (electronegativity) difference between the substituting atoms N/As and N/P is so large that CBM wave function localization appears around the impurity atoms [17] in the nitrogen dilute alloy limit (e.g., $GaP_{1-x}N_x$ for $x \to 0$). Consequently, even at finite compositions, the alloy CBM wave function is still localized around N atoms. If we draw spheres (radius = 1 Å) around each atom, we can calculate the weight (Q_{atom}) of $\psi_{\mathrm{CMB}}(\mathbf{r})^2$ inside each sphere.

TABLE I. Calculated projections $P_i(\mathbf{k}_{\mathrm{MR}})$ [Eq. (1)] of alloy state ψ_i. If $P_i(\mathbf{k}_{\mathrm{MR}}) \approx 1$, the state has approximated translational symmetry. N is the number of atoms in the supercell. w_{MR} is the majority representation weight, which is calculated as the sum of $P_i(\mathbf{k})$ around $\mathbf{k}_{\mathrm{MR}}$ (dashed line box shown in Fig. 4) from the $N = 32\,768$ supercells. The $N = 512$ results are an ensemble averaged over five random configurations. For the $N = 4096$ and $N = 32\,768$ systems, the effects of the ensemble average is insignificant.

Alloy	$\mathbf{k}_{\mathrm{MR}}$	$P_i(\mathbf{k}_{\mathrm{MR}})$ $N = 512$	$P_i(\mathbf{k}_{\mathrm{MR}})$ 4096	$P_i(\mathbf{k}_{\mathrm{MR}})$ 32 768	w_{MR}
$Ga_{0.7}Al_{0.3}As$	Γ(CBM)	0.839	0.900	0.914	0.918
	Γ(VBM)	0.978	0.921	0.743	0.958
$Ga_{0.4}Al_{0.6}As$	X(CBM)	0.998	0.983	0.900	0.980
	Γ(VBM)	0.965	0.929	0.783	0.953
$Ga_{0.5}In_{0.5}As$	Γ(CBM)	0.996	0.995	0.994	0.995
	Γ(VBM)	0.968	0.958	0.719	0.957
$GaAs_{0.5}N_{0.5}$	Γ(CBM)	0.549	0.545	0.537	0.543
	Γ(VBM)	0.050	0.006	0.001	0.014
$GaP_{0.875}N_{0.125}$	Γ(CBM)	0.314	0.359	0.262	0.310
	Γ(VBM)	0.725	0.058	0.004	0.051

For the $GaAs_{0.5}N_{0.5}$ system, we found [19] $Q_{\mathrm{N}}/Q_{\mathrm{As}} \approx 4$. [For the GaAlAs and GaInAs systems, both $Q_{\mathrm{GA}}/Q_{\mathrm{Al}}$ and $Q_{\mathrm{Ga}}/Q_{\mathrm{In}}$ are very close to 1.] The strong atom-type-charge-localization in the $GaAs_{0.5}N_{0.5}$ and $GaP_{0.875}N_{0.125}$ systems leads to a small (0.3–0.5) spectral projection $P_i(\mathbf{k}_{\mathrm{MR}})$ shown in Fig. 2 and Table I. The isosurface of $\psi^2_{\mathrm{CBM}}(\mathbf{r})$ is extended but irregular (spongelike), in strong contrast to that of case (i) (Fig. 1). This irregularity reflects the fact that ψ^2_{CBM} has a large chemical localization on the *randomly distributed* N atoms.

(iii) *No majority representation: The VBM of GaAsN and GaPN.*—While an impurity N atom in GaAs and GaP causes either a resonant state or a shallow bound state near the conduction band, an impurity As or P atom in GaN introduces a deep (~0.6 eV) bound state above the valence band maximum [17]. As a result, the VBM of GaAsN and GaPN is atomistically localized near a few (~20–50) atoms, as shown in the isosurface plot of Fig. 3. Consequently, there is no majority representation in $P_i(\mathbf{k})$, as shown in Fig. 3 and Table I.

(iv) *Strong majority representation with localization due to composition fluctuations: The VBM of GaAlAs and GaInAs.*—It is well known [3,4] that for a macroscopic alloy, the band tail states near the band edge are localized due to composition fluctuations. The composition fluctuation localization is weak, with its localization region containing tens of thousands of atoms. Figure 4 shows this situation for the VBM of $Ga_{0.4}Al_{0.6}As$ (the situation for VBM's of $Ga_{0.7}Al_{0.3}As$ and $Ga_{0.5}In_{0.5}As$ are very similar as shown in Table I). The majority representation peak in $P_{\mathrm{VBM}}(\mathbf{k})$ is evident, but unlike case (i), here it has a finite width of $\sim 2\pi/d_L$, where d_L is the localization size. As shown in the isosurface plot, the wave function is localized within a region containing ~100 000

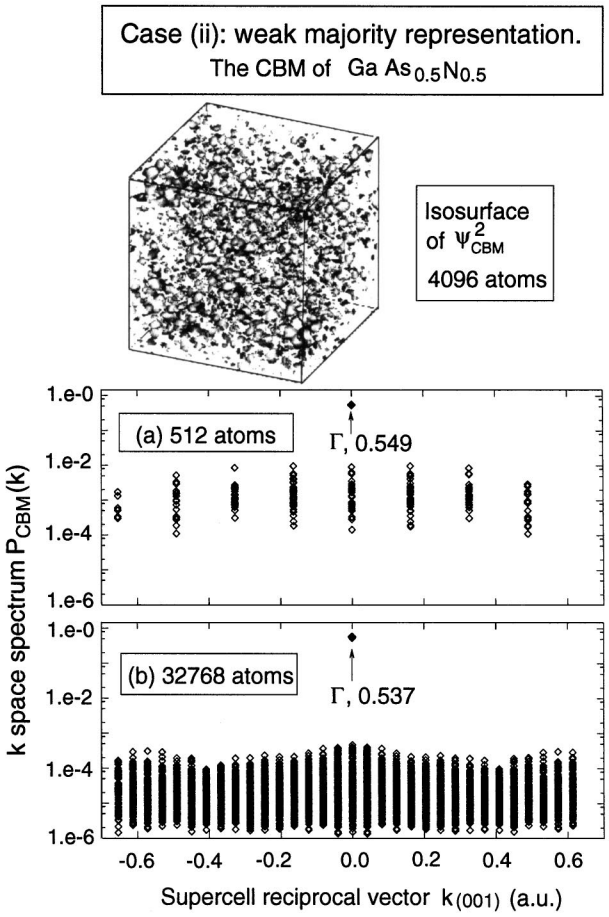

FIG. 2. Conduction band minimum state of $GaAs_{0.5}N_{0.5}$. See caption of Fig. 1 for details.

atoms corresponding to $d_L \sim 150$ Å. The isosurface has a cigar shape, oriented along the (111) direction, and having a long vs short axis ratio of ~3. The $P_{\mathrm{VBM}}(\mathbf{k}_{\mathrm{MR}})$ is 0.78 for the 32 768 atom supercell (Fig. 4) and 0.40 for the 2 million atom supercell. However, if we sum over $P_{\mathrm{VBM}}(\mathbf{k})$ within the $2\pi/d_L$ peak (dashed box in Fig. 4), the result comes back to 0.95, similar to the $P_{\mathrm{VBM}}(\mathbf{k}_{\mathrm{MR}})$ values for the smaller supercells, as listed in Table I. The total sum of this majority representation peak [instead of the single value $P_{\mathrm{VBM}}(\mathbf{k}_{\mathrm{MR}})$] is called the "majority representation weight" (w_{MR}), and is listed in Table I. One would expect also a localization due to composition fluctuation for the CBM states. However, we find that the $\mathbf{k}_{\mathrm{MR}} = \Gamma$ CBM states have a much larger localization size than their corresponding VBM states, due to much smaller electron effective masses compared to the hole effective masses.

There are a few implications to our results. In the case (i) of strong majority representation, alloy states can be classified in the language of Bloch states of the constituents. Average Green's function (AGF), CPA, and even VCA may be used, although the background part of $Q_i(\kappa)$ [with a total weight of $1 - P_i(\mathbf{k}_{\mathrm{MR}})$] ignored in VCA could contribute significantly to the

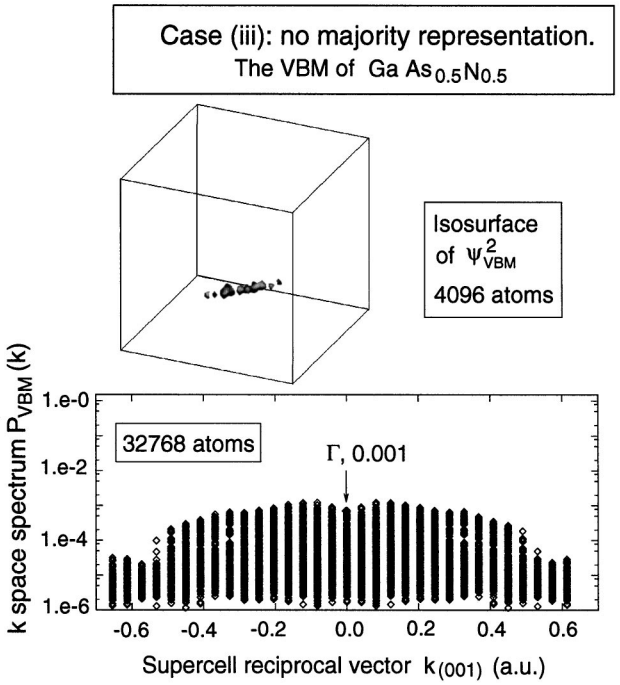

FIG. 3. Valence band maximum state of $GaAs_{0.5}N_{0.5}$. See caption of Fig. 1 for details.

"optical bowing." In the case (ii) of weak majority representation, the states can still be classified according to $\mathbf{k}_{MR}$. However, the VCA model clearly cannot be used, and it is questionable whether AGF and CPA can be used here in practice. The carrier transport [1], PL transition probability, and selection rules [5] can deviate severely from pure crystal behaviors. In the case (iii) of no majority representation, the wave functions are strongly localized, so it does not make sense to classify them using Bloch state notations [19] (e.g., Γ, X, L). As found in some recent calculations [19] and experiments [20], the "direct/indirect" transition in GaPN becomes very weak as N composition increases, mainly due to the strong localization of the VBM state. All the above theoretical models do not apply here. In the case (iv) of composition fluctuation localization, we find that the localized wave function has a particular smooth shape and orientational preference. This will affect the transports of the trapped excitons.

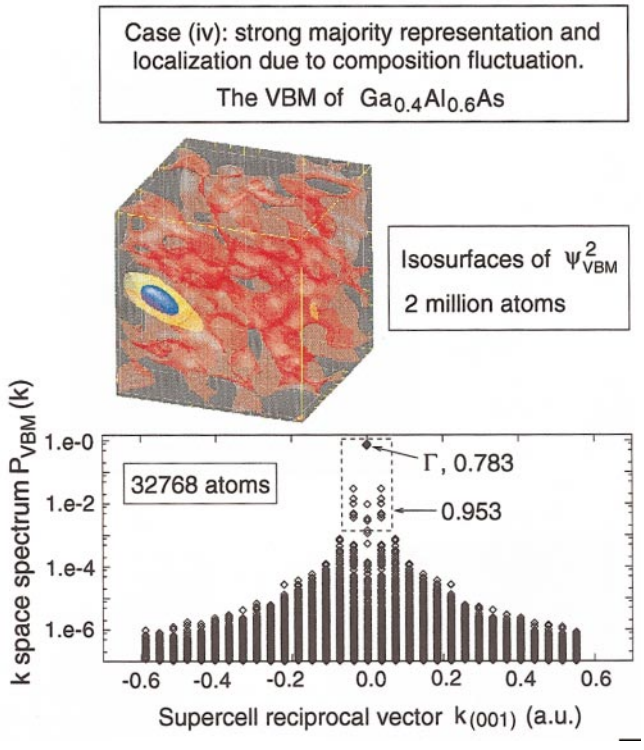

FIG. 4(color). Valence band maximum state of $Ga_{0.4}Al_{0.6}As$. The blue, yellow, and red isosurfaces encompass 10%, 20%, and 90% of the total wave function charges, respectively. The region inside the yellow isosurface contains about 20 000 atoms.

The authors thank J. C. Sturm for pointing out to us important references in this field. This work was supported by the U.S. Department of Energy, OER-BES, under Grant No. DE-AC36-83CH10093.

[1] V. Venkatarman *et al.*, Appl. Phys. Lett. **63**, 2795 (1993).
[2] L. C. Lenchyshyn *et al.*, Appl. Phys. Lett. **60**, 3174 (1992); L. C. Lenchyshyn *et al.*, J. Electron. Mater. **22**, 233 (1992).
[3] A. L. Efros and M. E. Raikh, in *Optical Properties of Mixed Crystals*, edited by R. J. Elliott and I. P. Ipatova (North-Holland, New York, 1988).
[4] S. Permogorov and A. Reznitsky, J. Lumin. **52**, 201 (1992).
[5] J. Weber and M. I. Alonso, Phys. Rev. B **40**, 5683 (1989).
[6] A. B. Almazov, *Electronic Properties of Semiconducting Solid Solutions* (Consultants Bureau, New York, 1968).
[7] A. B. Chen and A. Sher, *Semiconductor Alloys: Physics and Material Engineering* (Plenum Press, New York, 1995).
[8] L. Nordheim, Ann. Phys. (Leipzig) **9**, 607 (1931).
[9] L. W. Wang and A. Zunger, Phys. Rev. B **56**, 12 395 (1997).
[10] T. G. Dargam, R. B. Capaz, and B. Koiller, Phys. Rev. B **56**, 9625 (1997).
[11] R. J. Elliott *et al.*, Rev. Mod. Phys. **46**, 465 (1974).
[12] P. Soven, Phys. Rev. **156**, 809 (1967).
[13] R. H. Parmenter, Phys. Rev. **97**, 587 (1995); Phys. Rev. **104**, 22 (1956).
[14] L. W. Wang and A. Zunger, J. Chem. Phys. **100**, 2394 (1994).
[15] L. W. Wang, A. Franceschetti, and A. Zunger, Phys. Rev. Lett. **78**, 2819 (1997).
[16] K. A. Mader and A. Zunger, Phys. Rev. B **50**, 17 393 (1994).
[17] L. Bellaiche, S. H. Wei, and A. Zunger, Appl. Phys. Lett. **70**, 3558 (1997).
[18] J. L. Martins and A. Zunger, Phys. Rev. B **30**, 6217 (1984).
[19] L. Bellaiche, S. H. Wei, and A. Zunger, Phys. Rev. B **54**, 17 568 (1996); **56**, 10 233 (1997).
[20] J. N. Baillargeon *et al.*, Appl. Phys. Lett. **60**, 2540 (1992).